symmetry

MDPI

Article

Joint Optimal Planning of Flexible Resources in Distribution Networks Facing Multi-Dimensional Asymmetric Challenges

Saining Yin [1,*], Guowu Li [2], Xinsheng Ma [1], Zezhong Wang [2], Jin Zong [2], Weiyu Li [1], Ruoxuan Lu [3] and Jiali Wang [3]

[1] State Grid Jibei Electric Power Company Limited Electric Power Research Institute, Beijing 100000, China; gwjbdky_maxinsheng@163.com (X.M.); gwjbdlgs_liweiyu@163.com (W.L.)
[2] State Grid Jibei Electric Power Company Limited, Beijing 100054, China; gwjbdlgs_liguowu@163.com (G.L.); gwjbdlgs_wzz@163.com (Z.W.); gwjbdlgs_zongjin@163.com (J.Z.)
[3] School of Electrical and Information Engineering, Tianjin University, Tianjin 300072, China; lu_rx@tju.edu.cn (R.L.); wjl0830@tju.edu.cn (J.W.)
* Correspondence: gwjbdky_yinsaining@163.com; Tel.: +86-19930724987

Abstract

Modern distribution networks face dual challenges: extremely asymmetric spatial power flows caused by the high-penetration integration of distributed renewables under normal operating conditions and asymmetric system faults triggered by extreme weather such as blizzards under extreme conditions. To address these imbalances, this paper integrates distributed energy storage (DES) and soft open points (SOPs) as flexible resources to propose a two-stage joint optimal planning method that balances operational economy and resilience enhancement. First, by incorporating the spatiotemporal evolution trajectory and distance attenuation effects of blizzards, a multi-dimensional scenario sets characterizing asymmetric faults and normal source-load fluctuations are constructed. Second, a joint optimal planning model minimizing the total lifecycle cost is established. The progressive hedging algorithm is then adopted to decouple cross-scenario variables for efficient parallel solving. Verified on both the IEEE 33-node and large-scale 123-node systems, the coordinated planning strategy effectively avoids redundant investment in a single type of device. By establishing a symmetrical balance of flexible resources, the proposed method significantly reduces network losses and renewable curtailment during normal operation, while minimizing the amount of system load shedding under extreme asymmetric faults.

Keywords: distribution networks; symmetry/asymmetry; soft open points; distributed energy storage; resilience enhancement; optimal planning

Check for updates

Academic Editor: Vasilis K. Oikonomou

Received: 6 May 2026
Revised: 29 May 2026
Accepted: 1 June 2026
Published: 4 June 2026

Copyright: © 2026 by the authors. Licensee MDPI, Basel, Switzerland. This article is an open access article distributed under the terms and conditions of the Creative Commons Attribution (CC BY) license.

1. Introduction

In the development of new power systems, distribution networks, as the core carriers for distributed renewable energy and diverse load integration, are facing multiple asymmetry challenges arising from their physical structures and operating conditions. On the one hand, with the high-penetration integration of distributed photovoltaics, the source-load characteristics within the distribution network exhibit significant differentiation, leading to extremely unbalanced spatiotemporal power flow distributions. This spatial power asymmetry severely constrains the operational economy of the system and the local accommodation of renewable energy. On the other hand, the frequent occurrence of extreme disasters such as typhoons and blizzards in recent years has inflicted severe spatiotemporally asymmetric impacts on distribution networks, resulting in localized grid

fractures and large-scale power outages. Since distribution networks directly serve end-users, the lack of resilience can trigger widespread social impacts. Consequently, how to utilize optimal planning methods to enhance efficiency under asymmetric normal operating conditions and ensure the symmetrical balance and reliable supply of critical loads under asymmetric extreme faults has become a focus of current research [1–3].

Following the impact of asymmetric extreme disasters, the restoration and resilience enhancement process of distribution networks typically relies heavily on network reconfiguration. Reference [4] proposed a two-stage resilient restoration framework that performs intelligent partitioning and microgrid merging through network reconfiguration; Reference [5] established a distributionally robust resilience enhancement strategy to optimize active network reconfiguration schemes under extreme weather conditions; and Reference [4] employed a distributed stochastic programming approach to investigate the effectiveness of load redistribution through cross-regional network reconfiguration post-disaster. However, extreme meteorological disasters can inflict profound damage on the system topology, resulting in severe network asymmetry and islanded operating states. Relying solely on a single network reconfiguration to restore symmetrical balance is highly insufficient; other flexible regulation resources must be synergistically considered during the fault recovery process.

Soft open points (SOPs), by virtue of their precise power regulation and flexible control mode switching capabilities, enable cross-regional symmetrical power reconfiguration and fault isolation in distribution networks [6–8]. Meanwhile, distributed energy storage (DES) can not only alleviate issues such as power flow reversals and voltage limit violations under normal conditions but also provide asymmetric voltage support and restoration buffering for critical loads under fault scenarios [9]. The deep integration of these two resources to construct a flexibly interconnected distribution network can both ameliorate the asymmetry of spatial source-load distributions under normal scenarios and accelerate power supply restoration via rapid fault isolation and load transfer capabilities under extreme scenarios. This integration serves as a critical pathway to simultaneously balance normal flexible operation and extreme resilience enhancement.

Existing domestic and international research on the optimal configuration of distributed energy storage and flexible interconnection devices in distribution networks predominantly focuses on single-dimensional scenarios, either normal flexible economic operation or extreme resilience enhancement. Among configuration studies oriented toward normal operating scenarios, Reference [10] configured energy storage-integrated SOPs to reduce losses, improve voltage profiles, and enhance renewable energy accommodation levels. Reference [11] constructed a coordinated planning framework for SOPs and distributed photovoltaics, mitigating voltage violations and line overloads caused by the high penetration of renewable energy. Reference [12] optimized the configuration of distributed generation and mobile energy storage with the objective functions of minimizing distribution network investment and maintenance costs while maximizing social welfare. Reference [13] performed a coordinated planning of ESSs and SOPs considering demand response and voltage stability maintenance, which improved the efficiency of the distribution network and enhanced its flexibility and reliability.

Conversely, research concerning resilience enhancement largely focuses on post-disaster strategies and resource coordination. For instance, References [14–16] identified distributed generation as a crucial post-disaster resource and proposed system resilience metrics to quantitatively analyze distribution network resilience. Reference [17] proposed a resilient design strategy encompassing distributed generation deployment and an automated switch addition, constructing a two-stage stochastic mixed-integer linear programming model to characterize the entire fault-to-recovery process. Reference [18] provided an

SOP configuration method to bolster the disaster resistance capabilities of the distribution networks following typhoon landfalls. Reference [19] proposed a resilience enhancement method for distribution networks considering the configuration of SOPs and ESSs. These studies indicate that the coordinated configuration of distributed generation and SOPs can significantly elevate the recovery capability of critical loads and the continuity of power supply within the system under extreme events.

However, existing studies still exhibit two primary limitations. First, regarding planning objectives, the majority of research isolates economically flexible operation from extreme disaster resilient recovery, lacking a unified framework to evaluate the comprehensive lifecycle value of flexible resources in mitigating multiple asymmetric scenarios. Second, concerning energy storage modeling, most existing configuration studies treat ESSs purely as emergency support resources, making it difficult to holistically coordinate the symmetrical game and adaptive balance between the economic realization of daily energy storage operations and the resilient backup reserves required for extreme scenarios at the foundational model level [20].

To address the aforementioned issues, this paper proposes an optimal configuration method for distributed energy storage and flexible interconnection devices in distribution networks that considers both operational economy and resilience enhancement.

(1) By introducing the spatiotemporal evolution trajectory and distance attenuation effects of blizzard disasters, a line fault model depicting the spatiotemporal asymmetric evolution of disasters is established;
(2) An initial disaster-state coupling constraint for energy storage is introduced, strictly equating the available energy capacity at the exact moment of a line fault with the capacity at the corresponding moment during normal operation, thereby achieving a symmetrical game between its daily energy arbitrage and resilience enhancement;
(3) A joint planning framework coordinating normal operation and extreme resilience is established. The progressive hedging algorithm is utilized to efficiently decouple and solve massive asymmetric scenarios, thereby maximizing the comprehensive lifecycle benefits of the system.

2. Construction of Normal Operation Scenario Sets

Under normal operation, the primary uncertainties faced by distribution networks originate from the intermittency of distributed photovoltaic (PV) outputs and the spatiotemporal asymmetry of load demand fluctuations. To reasonably evaluate the operational economy of the system in response to the asymmetric distribution of sources and loads during the planning phase, this paper constructs a normal fluctuation scenario set based on historical operational data.

(1) PV and Load Error Distribution Models

Historical typical daily output and load baseline curves of the distribution network are extracted. The prediction error of PV output is fitted using a boundary-limited beta distribution, while the load prediction error is fitted using a normal distribution. Their stochastic scenario generation models are shown as follows:

$$\begin{aligned} P_{j,s,t}^{PV} &= P_{PV}^{base}(t) \cdot (1 + \Delta\mu_{PV}),\ \Delta\mu_{PV} \sim \text{Beta}(\alpha, \beta) \\ P_{j,s,t}^{load} &= P_{load}^{base}(t) \cdot (1 + \Delta\mu_{load}),\ \Delta\mu_{load} \sim N(0, \sigma^2) \end{aligned} \tag{1}$$

where $P_{j,s,t}^{PV}$,$P_{j,s,t}^{load}$ are the predicted available values of PV and load, respectively, for node j at time t under the generated scenario s.

(2) Scenario Sampling and Reduction

LHS is utilized to independently and uniformly generate a massive amount of matched PV and load samples within the probability distribution space. To balance computational accuracy and solution efficiency, the K-means clustering algorithm is subsequently employed to conduct scenario reduction on the initial samples. Ultimately, N_{norm} typical normal operation scenarios are generated, constituting the normal scenario set S_{norm}, with the occurrence probability of each typical scenario denoted as p_s.

3. Construction of Extreme Scenario Sets

3.1. Impact Mechanism of Blizzard Disasters on Distribution Networks

Taking blizzards as a representative extreme event, this paper constructs an extreme scenario set that accounts for complex spatiotemporal evolution characteristics, disaster intensities, and occurrence probabilities. Extreme blizzards are characterized by strong locality and dynamic migration over time, resulting in significant spatiotemporal asymmetry in the disaster impacts experienced by feeders at different spatial locations within the distribution network across different time periods. To accurately simulate this asymmetric evolution process, this section first establishes a spatiotemporal evolution model for distribution network line faults under blizzard disasters. Subsequently, based on this model, a Monte Carlo simulation considering multiple disaster intensities is utilized to generate the extreme scenario set.

- Blizzard Disaster Evolution Model Considering Spatiotemporal Characteristics

Based on the classical meteorological and fluid dynamics standard models for ice accretion on overhead lines, the classical cylindrical ice accretion model is extended into the spatiotemporal dimension by incorporating the spatiotemporal translation trajectory of the blizzard meteorological center [21]. The spatiotemporal translation trajectory of the blizzard meteorological center is introduced. Let the coordinates of the blizzard meteorological center at time t be ($x_c(t)$,$y_c(t)$), and the spatial geographic center coordinates of the distribution network feeder (i,j) be (x_{ij},y_{ij}). The spatial distance between the two at time t is d_{ij}. Based on the distance attenuation effect, the local dynamic snowfall rate $R_{ij}(t)$ and the local wind speed $v_{ij}(t)$ sustained by feeder (i,j) at time t are defined as follows, to quantify the spatially asymmetric stress caused by meteorological disasters:

$$\begin{aligned} R_{ij}(t) &= R_{max} \cdot \exp\left(-\frac{d_{ij}(t)^2}{2\sigma_R^2}\right) \\ v_{ij}(t) &= v_{max} \cdot \exp\left(-\frac{d_{ij}(t)^2}{2\sigma_v^2}\right) \end{aligned} \tag{2}$$

where R_{max} and v_{max} are the maximum snowfall rate and maximum wind speed at the blizzard center, respectively, σ_R and σ_v are the geometric spatial scale parameters of the meteorological impact, which can be obtained through spatial Gaussian fitting of meteorological observation data. This model quantifies the dynamic impact caused by the blizzard meteorological center on different spatial regions over time.

During the evolution process of the disaster, the ice and snow load on overhead lines does not form instantaneously but is accumulated through the forward integration of the continuous effects of local meteorological conditions. Assuming the disaster impact interval is [t_{start}, t_{end}], and combining the local dynamic snowfall rate $R_{ij}(t)$ and wind speed $v_{ij}(t)$, the accumulated equivalent ice and snow load per unit length on feeder (i,j) at time t, denoted as $M_{snow,ij}(t)$, is:

$$M_{snow,ij}(t) = \int_{t_{start}}^{t} \alpha(v_{ij}(\tau), \mu_{ij}) \cdot R_{ij}(\tau) d\tau \tag{3}$$

where α is the snow accretion conversion rate, considering the wind blow-off effect and the micro-topographical coefficient.

Assuming that the snow or ice uniformly accumulates on the outer surface of the conductor, it forms a hollow cylindrical sleeve. According to the geometric model of a cylinder's volume, there is a strict physical correspondence between the volume of snow accretion on the outer layer of the conductor and its weight as follows:

$$\rho_{snow}\pi\left[\left(H_{ij}(t)+\frac{D_{ij}}{2}\right)^2-\left(\frac{D_{ij}}{2}\right)^2\right]\cdot g=M_{snow,ij}(t) \tag{4}$$

The spatiotemporal equivalent snow thickness $H_{ij}(t)$ of feeder (*i*,*j*) at time t is as follows:

$$H_{ij}(t)=\sqrt{\frac{M_{snow,ij}(t)}{\rho_{snow}\pi g}+\left(\frac{D_{ij}}{2}\right)^2}-\frac{D_{ij}}{2} \tag{5}$$

where ρ_{snow} is the snow density, g is the gravitational acceleration, and D_{ij} is the outer diameter of the conductor.

- Line Failure Rate

Based on the classical line vulnerability model [22], considering the differences in service years and materials of lines at different spatial locations, specific spatial aging degradation rates ε_{ij} and physical load-bearing limits $H_{n,ij}$ are assigned to them. Accordingly, a line-breakage failure rate function $_{Pline,ij,l}(t)$ that dynamically evolves with time and space is established to characterize the physical probability of asymmetric breakage occurring in the network topology.

$$P_{line,ij}(t)=\begin{cases}\varepsilon_{ij}\left(A\cdot e^{\frac{H_{ij}(t)}{H_{n,ij}}}-B\right), H_{ij}(t)\le H_{n,ij}\\ 1, H_{ij}(t)>H_{n,ij}\end{cases} \tag{6}$$

where A and B are failure rate constants fitted based on historical disaster statistics.

3.2. Sampling-Based Generation of Extreme Scenario Sets

Referring to meteorological standards, this paper classifies the intensity of blizzard disasters into four levels (heavy snow, blizzard, severe blizzard, and extraordinary blizzard), denoted by the intensity level $l\in\{1,2,3,4\}$. Each intensity corresponds to different central meteorological parameters and historical occurrence probabilities. Based on the physical mechanism model in Section 3.1, this paper adopts a sequential Monte Carlo simulation method of "nested sub-scenarios": in each macroscopic disaster sampling, the four disaster intensities are compulsorily traversed. This accurately characterizes the uncertainty of disaster intensity and the spatiotemporal dynamic evolution of micro-faults in the distribution network. The specific generation steps are shown in Figure 1.

Step 1: Input the Weibull distribution parameters (α_T, β_T) for line repair duration, the maximum simulation time for extreme events T_E, and the predefined total number of macroscopic Monte Carlo samplings W. Initialize the scenario counter $w = 1$.

Step 2: Traverse the blizzard intensity levels l = 1,2,3,4. Extract the meteorological extreme values $R_{max,l}$ and $v_{max,l}$, as well as the occurrence probability p_l under this intensity.

(1) Disaster occurrence time: Assuming that the weather system's transit time and its extreme intensity are mutually independent, the random start time for this scenario is sampled as $t_{start,w,l} \sim U(1, T_{max_start})$.

(2) Disaster duration: Based on meteorological physical laws, the intensity and duration of a weather system are highly positively correlated. The disaster duration is defined as a conditional random variable dependent on the intensity l, characterized by a conditional lognormal distribution: $t_{start,w,l}$ ~ Lognormal($\mu_{ln}(l)$, ${\sigma_{ln}}^2(L)$. A higher intensity level l corresponds to a larger expected value of the distribution.

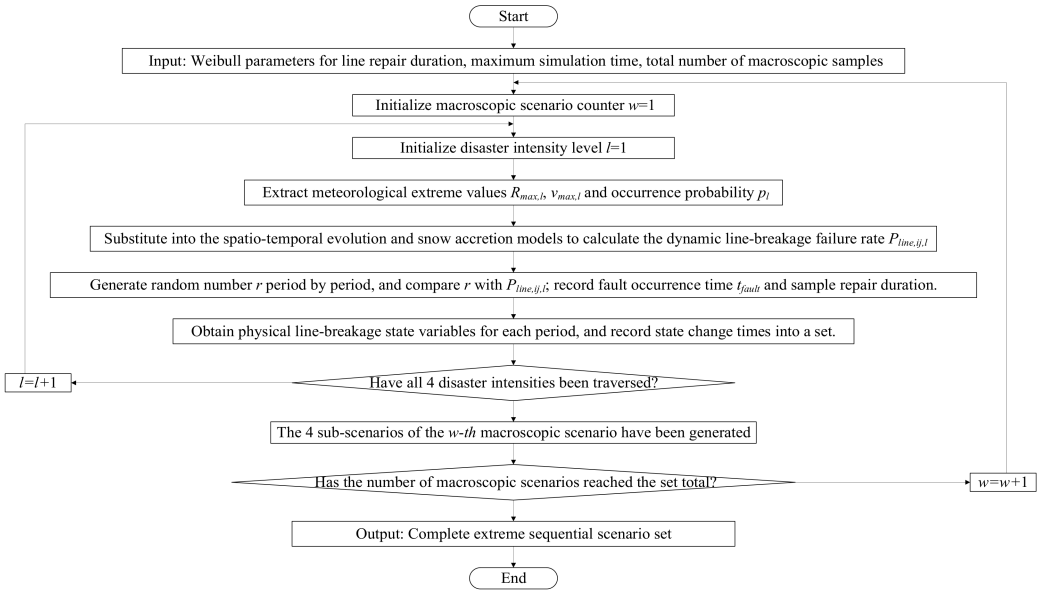


Figure 1. Flowchart of extreme scenario generation based on nested sequential Monte Carlo simulation.

Step 3: Based on the sampled time window [$t_{start,w,l}$, $t_{start,w,l} + T_{snow,w,l}$], substitute these into the spatiotemporal dynamic evolution model to calculate the local snowfall rate $R_{ij}(t)$ and wind speed $v_{ij}(t)$ for each line, which dynamically change over time and space.

Step 4: Adjust the lower limit of integration to the actual occurrence time of the disaster, and calculate the accumulated equivalent ice and snow load $M_{snow,ij}(t)$ at time t:

$$M_{snow,ij,l}(t) = \begin{cases} 0, t < t_{start,w,l} \\ \int_{t_{start,w,l}}^{t} \alpha(v_{ij,l}(\tau), \mu_{ij}) \cdot R_{ij,l}(\tau) d\tau, t \geq t_{start,w,l} \end{cases} \quad (7)$$

Substitute the intensity extreme values into the spatiotemporal dynamic evolution model and the forward cumulative snow accretion model to calculate the dynamic line-breakage failure rate $P_{line,ij,l}(t)$ for each line, which changes with time under scenario w and intensity l.

Step 5: Evaluate all lines in the distribution network period by period. At time t, generate a uniformly distributed random number r. If $r < P_{line,ij,l}(t)$, and the line has not yet broken, record this moment as the fault occurrence time $t^D_{ij,w,l} = t$. Simultaneously, sample to obtain the emergency repair and restoration duration for this line $t^R_{ij,w,l}$~Weibull(α_T, β_T).

Step 6: Obtain the physical line-breakage state variables of line (i,j) at each time period under scenario w and intensity l, and record the moments of line state changes into the corresponding set $T^{Tr}_{w,l}$:

$$f_{ij,w,l}(t) = \begin{cases} 1, t^D_{ij,w,l} \leq t \leq \min\left\{t^D_{ij,w,l} + t^R_{ij,w,l} - 1, T_E\right\} \\ 0, else \end{cases} \quad (8)$$

Step 7: Determine whether all four disaster intensities have been traversed. If not, let $l = l + 1$ and return to Step 2; if traversed completely, it indicates that all four sub-scenarios for the w scenario have been generated.

Step 8: Determine whether the scenario counter w has reached the total number W. If not, let $w = w + 1$ and return to Step 2; otherwise, output the complete extreme sequential scenario set Ω_{snow}.

4. Two-Stage Joint Planning Model Considering Economic Benefits and Resilience Enhancement

This paper establishes a mixed-integer nonlinear optimal planning model aimed at minimizing the total lifecycle economic cost of planning and operation. The solution process of the planning model is shown in Figure 2. By configuring flexible interconnection devices and energy storage, it aims to break the limitations of spatiotemporally asymmetric operations in distribution networks, enhancing operational economy under normal scenarios and resilience under extreme scenarios, thereby maximizing the comprehensive benefits of flexible resources across multiple asymmetric scenarios.

$$\min C^{total} = C^{inv} + M_N C^{flex} + M_E C^{res} \tag{9}$$

where M_N is the annualized weight of normal scenarios, taken as 365 based on the days in a year; M_E is the annualized weight of extreme scenarios, which depends on the average annual occurrence frequency of extreme events such as blizzards.

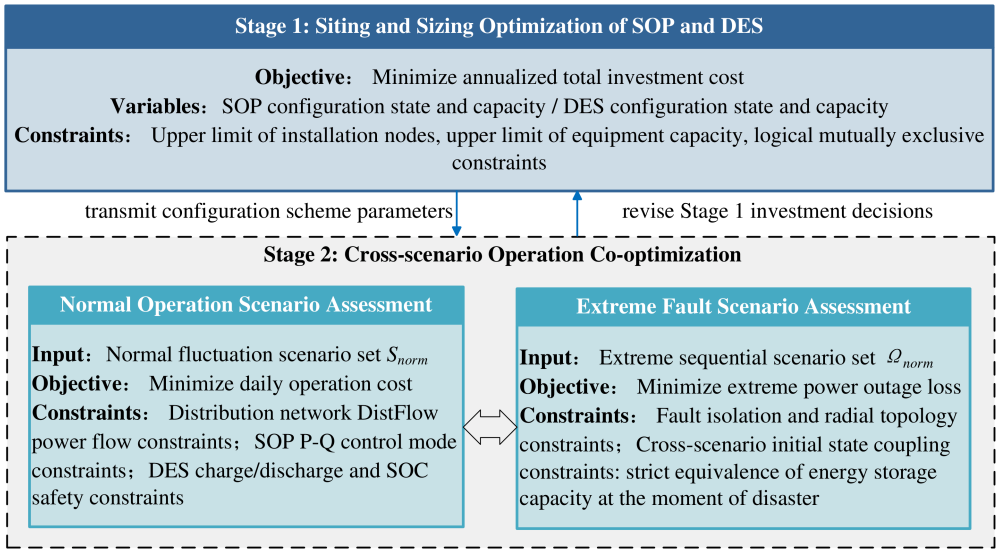


Figure 2. Two-stage collaborative planning framework.

4.1. Investment Model for Siting and Sizing of SOP and DES

The first stage independently optimizes the installation locations and capacities of the devices within the distribution network. SOPs are deployed at candidate tie lines between adjacent feeders to achieve the reconfiguration and balance of spatially asymmetric power flows; DES, as an independent AC resource, is directly connected to candidate AC nodes within the distribution network to provide symmetrical temporal-shift support in the time dimension.

$$C^{inv} = \sum_{(i,j)\in\Omega_{TS}} y_{ij}^{SOP} \Gamma c_{SOP} S_{ij}^{SOP,cap} + \sum_{j\in\Omega_N} y_j^{DES} \Gamma (c_P P_j^{DES,cap} + c_E E_j^{DES,cap}) \tag{10}$$

where $y_{ij}^{SOP}, y_j^{DES} \in \{0,1\}$ are the siting state decision variables for SOP and DES, respectively; Ω_{TS} is the set of candidate tie lines between transformer areas; Ω_N is the set of candidate AC nodes within transformer areas; c_{SOP}, c_P, c_E are the corresponding unit costs;

Γ is the annualized capital recovery factor; and $S_{ij}^{SOP,cap}$, $P_j^{DES,cap}$, $E_j^{DES,cap}$ are the upper bounds of the capacity configured in the first stage.

The planning constraint for SOP is:

$$\sum_{(i,j)\in E_{NOP}} y_{ij}^{SOP} \le N_{SOP} \tag{11}$$

where E_{NOP} is the set of candidate tie lines that are normally open; N_{SOP} is the upper limit for the number of SOPs to be configured. This equation restricts SOPs from being configured exclusively at tie lines to replace normally open tie switches, and their quantity is limited.

The planning constraint for DES is as follows:

$$\sum_{i\in V_{DES}} y_i^{DES} \le N_{DES} \tag{12}$$

where V_{DES} is the set of candidate AC nodes for energy storage integration within the transformer areas; N_{DES} is the upper limit for the number of distributed energy storage units to be configured. This equation limits the maximum number of installation nodes for energy storage devices in the system.

4.2. Normal Operation Model Considering Economy

The objective of normal operation is to fully utilize the cross-regional transfer capability of SOPs and the time-shifting capability of DES to correct the extremely asymmetric spatial distribution of power flows caused by the high penetration of PV integration, promoting PV accommodation and smoothing the spatiotemporal asymmetry of system fluctuations.

$$C^{flex} = \sum_{s\in S_{norm}} p_s \sum_{t=1}^{24} \left(c_{grid} P_{grid,s,t} + c_{loss} P_{loss,s,t} + c_{curt} P_{curt,s,t} + \lambda_v \sum_{j\in B} |\Delta U_{j,s,t}| \right) \tag{13}$$

where $P_{grid,s,t}$ represents the power purchased from the main grid; $P_{loss,s,t}$ represents the active power network loss of the lines; $P_{curt,s,t}$ represents the PV curtailment amount; $\Delta U_{j,s,t}$ represents the magnitude of the nodal voltage deviation; and c and λ_v represents the corresponding economic or penalty coefficients.

(1) Distribution Network Power Flow Constraints

This paper adopts the DistFlow model to construct power flow constraints, including distribution network power flow balance constraints considering the integration of soft open points, nodal voltage constraints, line current constraints, and line power flow constraints. The specific expressions can be found in Reference [23].

Under normal scenarios, the output of distributed renewable energy must satisfy the following equation:

$$\begin{cases} 0 \leqslant P_{j,s,t}^{\mathrm{REG}} \leqslant P_{j,s,t}^{\mathrm{PREG}} \\ 0 \leqslant Q_{j,s,t}^{\mathrm{REG}} \leqslant Q_{j,s,t}^{\mathrm{PREG}} \end{cases} j \in B_{\mathrm{DG}} \tag{14}$$

where $P_{j,s,t}^{\mathrm{REG}}$ and $Q_{j,s,t}^{\mathrm{REG}}$ are the actual active and reactive power outputs of the distributed renewable energy at node j, time t, under scenario s, respectively. $P_{j,s,t}^{\mathrm{PREG}}$ and $Q_{j,s,t}^{\mathrm{PREG}}$ are the predicted upper limits of available active and reactive power of the distributed renewable energy at node j, time t, under scenario s, respectively. B_{DG} is the set of nodes integrated with distributed renewable energy in the distribution network.

(2) SOP Operation Constraints

In fault-free normal scenarios, the SOP configured at the tie line (*i*,*j*) operates in P-Q control mode. Its active power balance and capacity constraints are as follows:

$$\begin{aligned} P_{i,s,t}^{SOP} + P_{j,s,t}^{SOP} + A_{SOP} \cdot \left(\left|P_{i,s,t}^{SOP}\right| + \left|P_{j,s,t}^{SOP}\right|\right) = 0 \\ \left(P_{i,s,t}^{SOP}\right)^2 + \left(Q_{i,s,t}^{SOP}\right)^2 \le \left(S_{ij}^{SOP,cap}\right)^2 \\ \left(P_{j,s,t}^{SOP}\right)^2 + \left(Q_{j,s,t}^{SOP}\right)^2 \le \left(S_{ij}^{SOP,cap}\right)^2 \end{aligned} \tag{15}$$

where $P_{i,s,t}^{SOP}$ and $Q_{i,s,t}^{SOP}$ are the active and reactive power injected by the SOP converter at the *i*-side node; A_{SOP} is the internal active power loss coefficient of the SOP; $S_{ij}^{SOP,cap}$ is the apparent capacity upper limit of the SOP configured at the tie line (*i*,*j*).

To ensure computational efficiency and global optimality, a second-order convex relaxation technique is employed to transform the SOP constraints into a second-order cone programming model. Based on the principle of equivalent second-order cone transformation, the loss constraint inequalities are converted into standard second-order cone constraints, and the capacity constraints are equivalently transformed into rotated second-order cone constraints.

$$\begin{aligned} \left\| \begin{array}{c} 2\sqrt{A_j^{SOP}} P_{j,t,s}^{SOP} \\ 2\sqrt{A_j^{SOP}} Q_{j,t,s}^{SOP} \\ P_{j,t,s}^{loss} - 1 \end{array} \right\|_2 \le P_{j,t,s}^{loss} + 1 \\ \left(P_{j,t,s}^{SOP}\right)^2 + \left(Q_{j,t,s}^{SOP}\right)^2 \le 2 \frac{S_{i,j}^{SOP}}{\sqrt{2}} \frac{S_{i,j}^{SOP}}{\sqrt{2}} \end{aligned} \tag{16}$$

(3) Energy Storage Operation Constraints

DES undergoes charge and discharge dispatch under normal operation. Its physical power constraints and energy evolution constraints are as follows:

$$\begin{aligned} & 0 \le P_{j,s,t}^{ch} \le u_{j,s,t}^{ch} P_j^{DES,cap},\ 0 \le P_{j,s,t}^{dis} \le u_{j,s,t}^{dis} P_j^{DES,cap} \\ & u_{j,s,t}^{ch} + u_{j,s,t}^{dis} \le 1,\ P_{j,s,t}^{DES} = P_{j,s,t}^{dis} - P_{j,s,t}^{ch} \\ & E_{j,s,t}^{DES} = E_{j,s,t-1}^{DES} + \eta^{ch} P_{j,s,t}^{ch} \Delta t - \frac{P_{j,s,t}^{dis}}{\eta^{dis}} \Delta t \\ & SOC_{min} \le \frac{E_{j,s,t}^{DES}}{E_j^{DES,cap}} \le SOC_{max} \end{aligned} \tag{17}$$

where $P_{j,s,t}^{ch}$ and $P_{j,s,t}^{dis}$ represent the actual charging and discharging power of the energy storage; $u_{j,s,t}^{ch}$ and $u_{j,s,t}^{dis}$ are the charging and discharging state indicators of the energy storage (0–1 binary variables, restricting simultaneous charging and discharging); $P_j^{DES,cap}$ and $E_j^{DES,cap}$ represent the maximum charge/discharge power limit and the rated capacity of the configured energy storage; and SOC_{min} and SOC_{max} are the safe lower and upper limits of the state of charge set to ensure battery life.

4.3. Fault Restoration Model for Resilience Enhancement in Extreme Scenarios

Under extreme blizzard scenarios, the distribution network suffers from asymmetric physical stress impacts leading to localized main grid outages, and the system objective shifts to minimizing the penalty loss of critical load shedding during the islanded period, resulting from topologically asymmetric breakage.

$$C^{res} = \sum_{w=1}^{W} p_w \sum_{l=1}^{4} p_l \sum_{t \in T_{w,l}^T r} \sum_{j \in B} \omega_j \cdot c_{voll} \cdot P_{shed,j,w,l,t} \tag{18}$$

where ω_j and c_{voll} represent the importance weight of node j and the unit value of the lost load penalty coefficient, respectively; $P_{shed,j,w,l,t}$ represents the actual amount of active and reactive load shed at node j at time t under a specific extreme scenario.

(1) Distribution Network Power Flow Constraints in Extreme Scenarios

The distribution network power flow constraints include power flow balance constraints of the distribution network considering the integration of soft open points, the relationship constraints between voltage and line power flow based on the Big-M method, nodal voltage constraints, and line power flow constraints considering the connectivity state of the lines. Their specific mathematical expressions can be found in Reference [24].

Under extreme scenarios, PV participates in post-disaster restoration in the form of conventional distributed generation. However, affected by the blizzard, if a power outage fault occurs at node j where the PV is located, its output is forced to zero.

$$0 \le P_{j,w,t}^{PV_act} \le P_{j,w,t}^{PV_predict}(1 - n_{j,w,t}) \tag{19}$$

$P_{j,w,t}^{PV_act}$ and $P_{j,w,t}^{PV_predict}$ refer to the actual dispatched output and the predicted theoretical output of the PV under extreme scenarios, respectively.

Under extreme scenarios, the load may face the risk of load shedding and must satisfy the following constraints:

$$\begin{aligned} 0 \le P_{shed,j,w,t} \le P_{j,w,t}^{load} \\ 0 \le Q_{shed,j,w,t} \le Q_{j,w,t}^{load} \end{aligned} \tag{20}$$

(2) Fault Isolation Constraints under Extreme Scenarios

Let Ω_{SS} be the set of normally closed sectionalizing switch lines, and Ω_{TS} be the set of normally open tie switch lines. Introduce the switch action state variable $s_{ij,w,t} \in \{0,1\}$ and the line connectivity state variable $c_{ij,w,t} \in \{0,1\}$. The physical state of normal sectionalizing switches is locked as closed; only normally open tie switches are allowed to perform closing reconfiguration operations.

$$\begin{aligned} &s_{ij,w,t} = 1 \ (i,j) \in \Omega_{SS} \\ &s_{ij,w,t} \in \{0,1\} \ (i,j) \in \Omega_{TS} \\ &s_{ij,w,t} \le 1 - y_{ij}^{SOP} \ (i,j) \in \Omega_{TS} \end{aligned} \tag{21}$$

A line fault will directly cause the nodes connected to both ends of the line to be affected by the fault and lose the power supply support from the main grid.

$$\begin{aligned} &n_{j,w,t} \ge f_{ij,w}(t) \ i \in \delta(j) \cup \pi(j) \\ &n_{i,w,t} \le \sum_{j \in \delta(i) \cup \pi(i)} f_{ij,w}(t) \end{aligned} \tag{22}$$

where $f_{ij,w}(t)$ is the physical line-breakage fault state variable of line (i,j) under disaster impact (one indicates the line has broken); $n_{j,w,t}$ is the state variable of node j experiencing power outage due to the fault impact (one indicates affected and losing power supply).

Switch action constraints:

$$\begin{aligned} &c_{ij,w,t} \le s_{ij,w,t} \ (i,j) \in (\Omega_{SS} \cup \Omega_{TS}) \\ &c_{ij,w,t} \le 1 - f_{ij,w}(t) \ (i,j) \in \Omega_L \\ &c_{ij,w,t} \ge s_{ij,w,t} - f_{ij,w}(t) \ (i,j) \in (\Omega_{SS} \cup \Omega_{TS}) \end{aligned} \tag{23}$$

(3) SOP Fault Isolation and Support Model under Extreme Scenarios

Based on the aforementioned capacity boundaries, the SOP under extreme faults is subject to additional disaster response and grid-forming support constraints: If a node on one side of the tie line where the SOP is located is affected by a fault, the converter on that side must be immediately physically blocked; simultaneously, the converter on the normal side can switch to V-f control mode to support the island voltage.

$$\begin{gathered} -S_{ij}^{SOP,cap}(1-n_{i,w,l,t}) \le P_{i,w,l,t}^{SOP} \le S_{ij}^{SOP,cap}(1-n_{i,w,l,t}) \\ -S_{ij}^{SOP,cap}(1-n_{j,w,l,t}) \le P_{j,w,l,t}^{SOP} \le S_{ij}^{SOP,cap}(1-n_{j,w,l,t}) \\ U_{set}^{min} \le U_{i,w,l,t} \le U_{set}^{max} \end{gathered} \tag{24}$$

where U_{set}^{min} and U_{set}^{max} represent the upper and lower limits of node voltage safety control when the SOP provides V-f support in the islanded state.

(4) Energy Storage Model under Extreme Scenarios

Under fault conditions, the DES switches to the emergency backup mode. Based on the aforementioned normal charge and discharge formulas, it is necessary to add physical self-protection isolation and critical disaster initial state coupling constraints. First, if the AC node where the DES is located experiences a short-circuit power outage due to a line breakage, the DES initiates self-protection blocking, and its active charge and discharge power are forced to zero:

$$\begin{gathered} 0 \le P_{j,w,l,t}^{ch} \le u_{j,w,l,t}^{ch} P_j^{DES,cap}(1-n_{j,w,l,t}) \\ 0 \le P_{j,w,l,t}^{dis} \le u_{j,w,l,t}^{dis} P_j^{DES,cap}(1-n_{j,w,l,t}) \end{gathered} \tag{25}$$

Secondly, a cross-scenario symmetric coupling constraint for the disaster's initial state is introduced. To achieve an adaptive game between normal economic dispatch and extreme emergency backup, this paper applies a strict equality constraint to couple the initial available energy of the energy storage at the moment an asymmetric line breakage fault occurs in a specific extreme scenario with its corresponding energy at the exact same moment in the normal operation scenario. This mathematically constructs a symmetrical mapping relationship between daily operational states and extreme disaster states:

$$E_{j,w,l,t_{w,l}^D}^{DES} = E_{j,s,t_{w,l}^D}^{DES} \tag{26}$$

where $t_{w,l}^D$ represents the initial moment when a line-breakage fault occurs under extreme scenarios.

(5) Radial topology constraints for restoring symmetrical power supply under extreme scenarios

After the occurrence of an asymmetric fault, network reconfiguration transfers loads by closing tie switches, attempting to maximally restore the system's power supply symmetry and balance, but the formation of the closed-loop networks must be prevented. A single-commodity flow graph theory algorithm is introduced to construct a virtual connected tree model, ensuring the topology remains radial:

$$\begin{gathered} \sum_{(i,j)\in E} c_{ij,w,t} = N_B - |Sub| - \sum_{j\in B} \gamma_{j,w,t} \\ \gamma_{j,w,t} \le \sum_{i\in\pi(j)} (1-c_{ij,w,t}) + \sum_{k\in\delta(j)} (1-c_{jk,w,t}) \\ -M\cdot c_{ij,w,t} \le F_{ij,w,t} \le M\cdot c_{ij,w,t} \\ \sum_{k\in\delta(j)} F_{jk,w,t} - \sum_{i\in\pi(j)} F_{ij,w,t} = \begin{cases} W_{j,w,t}, & j\in\{Sub\} \\ \gamma_{j,w,t}W_{j,w,t}-1, & j\notin\{Sub\} \end{cases} \end{gathered} \tag{27}$$

where $\gamma_{j,w,t}$ is a state variable indicating whether node j becomes the root node of an islanded virtual power source (one indicates becoming a root node); N_B and Sub are the total number of system nodes and the number of main grid (substation) root nodes, respectively; $F_{ij,w,t}$ is the virtual commodity flow introduced on line (i,j); M is a sufficiently large positive real number set in the Big-M method; and $W_{j,w,t}$ is the virtual load demand parameter corresponding to node j in the graph theory algorithm.

The prerequisite for a node to become the root node of an islanded virtual power source is that the node itself is configured with energy storage, or it is connected via lines to SOP equipment capable of providing *V*-*f* support:

$$\gamma_{j,w,t} \le y_j^{DES} + \sum_{k \in \delta(j) \cup \pi(j)} y_{jk}^{SOP} \; j \in B \setminus \{Sub\} \tag{28}$$

5. Model Solution Process Based on the Progressive Hedging Algorithm

In the two-stage model established in this paper, normal economic operation and extreme fault recovery exhibit profound asymmetry in their objectives and constraints. To address the challenge of cross-scenario variable coupling under a massive number of unanticipated scenarios, this paper adopts the progressive hedging (PH) algorithm to relax and decouple the cross-scenario symmetrically coupled variables, enabling efficient parallel solving of the model.

The core philosophy of the PH algorithm lies in breaking the information asymmetry and decision-making silos between scenarios: first, it allows each scenario to relax constraints and independently optimize under asymmetric operating conditions; subsequently, it calculates the weighted average expected solution across all scenarios. By introducing linear and quadratic penalty terms, the algorithm forces the asymmetric private decisions of each independent scenario to gradually converge toward a global consensus through iterations, until all scenarios achieve complete symmetry and consistency in their configuration schemes.

The specific steps of the solution process are as follows:

Step 1: Algorithm initialization. Set the iteration counter $k = 0$. Initialize the augmented Lagrangian penalty factor $\rho > 0$. Initialize the Lagrangian multiplier vectors for all scenarios to zero, i.e., $\boldsymbol{\omega}_s^{(0)} = \mathbf{0}, \boldsymbol{\omega}_{w,l}^{(0)} = \mathbf{0}$. Set the convergence tolerance threshold ε.

Step 2: Solve the initial independent subproblems in parallel. Temporarily remove the cross-scenario common decision equality constraints. For each normal operating scenario and each extreme sub-scenario, independently call the solver to solve its own single-scenario optimization problem. After solving, extract the private decision solutions considered optimal by each respective scenario: $X_s^{(0)}, X_{w,l}^{(0)}$.

Step 3: Calculate the global weighted average expectation. Based on the historical occurrence probabilities or sampling weights of each scenario, calculate the global average expected decision scheme $\overline{\boldsymbol{X}}^{(k)}$ at the current k-th iteration:

$$\overline{\boldsymbol{X}}^{(k)} = \frac{M_N \sum_s p_s \boldsymbol{X}_s^{(k)} + M_E \sum_w \sum_l p_w p_l \boldsymbol{X}_{w,l}^{(k)}}{M_N + M_E} \tag{29}$$

Step 4: Convergence check. Calculate the variance between all single-scenario private decisions and the global average decision $\Delta^{(k)}$:

$$\Delta^{(k)} = M_N \sum_s p_s ||\boldsymbol{X}_s^{(k)} - \overline{\boldsymbol{X}}^{(k)}||^2 + M_E \sum_w \sum_l p_w p_l ||\boldsymbol{X}_{w,l}^{(k)} - \overline{\boldsymbol{X}}^{(k)}||^2 \tag{30}$$

If the dispersion is $\Delta^{(k)} \leq \varepsilon$, it indicates that all scenarios have reached a completely consistent decision configuration under strict penalties, satisfying the non-anticipativity constraints. The algorithm converges and terminates the loop, outputting the final joint configuration scheme $X^* = \overline{X}^{(k)}$. If $\Delta^{(k)} \geq \varepsilon$, proceed to Step 5 to prepare for the next iteration.

Step 5: Update Lagrangian multipliers. For those scenarios that deviate from the global consensus $\overline{X}^{(k)}$, increase their Lagrangian penalty multipliers:

$$\omega_s^{(k+1)} = \omega_s^{(k)} + \rho(X_s^{(k)} - \overline{X}^{(k)}), \omega_{w,l}^{(k+1)} = \omega_{w,l}^{(k)} + \rho(X_{w,l}^{(k)} - \overline{X}^{(k)}) \quad (31)$$

Step 6: Construct and re-solve the augmented Lagrangian single-scenario subproblems. Introduce the penalty mechanism into the objective functions of every single scenario, forcing them to consider moving toward the global consensus while pursuing the minimization of their own operating costs. Let the iteration counter $k = k + 1$. For solving the subproblem of normal scenario s, the following equation is used:

$$\min C_s^{inv} + C_s^{flex} + (\omega_s^{(k)})^T X_s + \frac{\rho}{2}||X_s - \overline{X}^{(k-1)}||^2 \quad (32)$$

Subject to the physical constraints of normal operation, solve to obtain the new $X_s^{(k)}$.

For solving the subproblem of extreme scenarios, the following equation is used:

$$\min C_{w,l}^{inv} + C_{w,l}^{res} + (\omega_{w,l}^{(k)})^T X_{w,l} + \frac{\rho}{2}||X_{w,l} - \overline{X}^{(k-1)}||^2 \quad (33)$$

Subject to the physical constraints of extreme fault restoration, solve to obtain the new $X_{w,l}$. Once all subproblems are solved in parallel, return to Step 3.

6. Case Study Analysis

6.1. Case Study Setup

This paper uses the IEEE 33-node system for case study testing. The topology of the IEEE 33-node system is shown in Figure 3. The system contains 32 normally closed sectionalizing switch lines and five normally open tie lines. These five tie lines serve as candidate installation locations for SOPs. The candidate integration nodes for distributed energy storage (DES) are set at the terminal ends of the system or heavily loaded nodes (Nodes 21, 17, 24, and 32). The base voltage level of the test system is 12.66 kV, the safe magnitude range for node voltage is set to [0.95, 1.05] p.u., and the total normal load of the system is 3.715 MW + j2.300 Mvar.

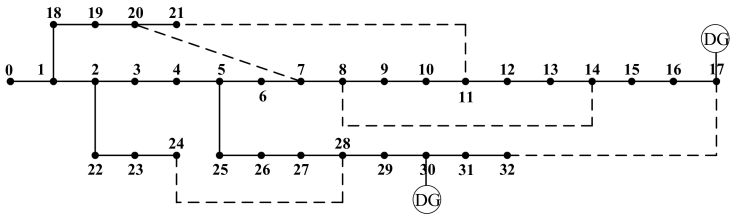


Figure 3. Topology of the IEEE 33-node system.

Two photovoltaic units are integrated into the distribution network, with a total rated capacity of 0.6 MW for the distributed renewable energy units. Under extreme blizzard scenarios, when the node is not affected by line-breakage faults where it is located, the distributed renewable energy participates in the restoration operation of the distribution network in the form of a conventional distributed generation.

Regarding the construction of the normal operation scenario set, one year of historical actual operation data for PV and load in a typical region is adopted. Following the previously described method, the probability distribution parameters of random fluctuation factors for the four seasons (spring, summer, autumn, and winter) are extracted. Based on this, Latin hypercube sampling and K-means clustering are utilized to generate 20 typical normal scenarios for economic operation optimization. Regarding the construction of the extreme scenario set, based on local historical meteorological statistics, the average annual occurrence probability of extreme blizzard events is established. Using Monte Carlo sampling, an extreme scenario set comprising a total of 20 scenarios that consider spatiotemporal characteristics is generated.

6.2. Case Setup and Result Analysis

To verify the superiority of the coordinated configuration of SOPs and distributed energy storage in correcting the normal asymmetric operation of the distribution network and coping with the asymmetric impacts of extreme disasters, this paper establishes four different configuration schemes for comparative analysis based on the IEEE 33-node system.

Scheme 1: No flexible resources are present in the distribution network; post-disaster restoration relies solely on closing tie switches for network reconfiguration and load transfer.

Scheme 2: Only SOPs are optimally configured at the candidate locations in the distribution network.

Scheme 3: Only DES is optimally configured at the candidate locations in the distribution network.

Scheme 4: Both SOPs and DES are optimally configured at the candidate locations in the distribution network.

Under the unified system data and scenario sets, the progressive hedging algorithm is used to optimize the above four schemes. The obtained siting and sizing results are shown in Table 1, and the economic costs of the four schemes are shown in Table 2.

Table 1. Optimal configuration results under different schemes.

Configuration	SOP			DES		
		Location	Capacity /(kVA)		Location	Capacity /(kWh)
Scheme 1	/	/	/		/	/
Scheme 2	1 2 3	11, 21 24, 28 17, 32	250 240 310	/	/	/
Scheme 3	/	/	/	1 2 3	17 24 32	800 800 800
Scheme 4	1 2	7, 20 17, 32	240 320	1 2	17 32	500 800

Comparing the resource siting and sizing results and operation costs of the four schemes, it can be seen that the configuration of a single flexible resource often leads to redundant equipment investment and limited operational benefits. Due to the lack of flexible regulation means, Scheme 1 incurs extremely high penalties for network loss and PV curtailment. In Scheme 2 and Scheme 3, the system is forced to increase the configuration capacity of individual devices to compensate for the singularity of spatial transfer or

temporal shifting capabilities. In contrast, Scheme 4 proposed in this paper achieves the spatiotemporal-coordinated joint configuration of SOP and DES. This coordinated configuration not only avoids excessive redundant investment in a single device but also reduces the system's network loss and PV curtailment penalties at a more reasonable configuration cost, achieving the optimization of economic operation under the symmetrical balance of spatiotemporal resources.

Table 2. Cost comparison of different configuration strategies (Unit: $\times 10^4$ CNY).

Configuration	Cost				
	Configuration	Network Loss	PV Curtailment	Load Shedding	Total
Scheme 1	0	28.14	16.12	6.26	50.52
Scheme 2	5.48	15.20	10.50	4.80	35.98
Scheme 3	7.20	22.10	11.30	3.90	44.50
Scheme 4	9.88	10.05	6.44	2.64	29.01

From the perspective of resilience performance under extreme disasters and the comprehensive system cost over the entire life cycle, Scheme 4 enables energy storage to achieve a symmetrical game and adaptive balance between daily arbitrage and disaster backup. The energy reserved before the disaster, combined with the cross-regional symmetrical power flow regulation capability of the SOP, significantly reduces the extreme load-shedding penalty. Overall, although the configuration cost of Scheme 4 is the highest, the economic losses it recovers during normal operation and extreme disasters far exceed the hardware investment. This fully proves that the coordinated configuration strategy effectively balances the operational economy and resilience enhancement capability.

The macroscopic average annual occurrence probability of extreme disasters directly determines the system's investment weight allocation between "normal operational economy" and "extreme scenario security". The baseline case in this paper sets the macroscopic average annual occurrence probability of blizzards to 0.05. To verify the adaptability of the configuration strategy in regions with different climate risks, the probability is gradually increased from 0.01 to 0.10. The coordinated configuration results of flexible resources and the cost variation trends are shown in the Figure 4.

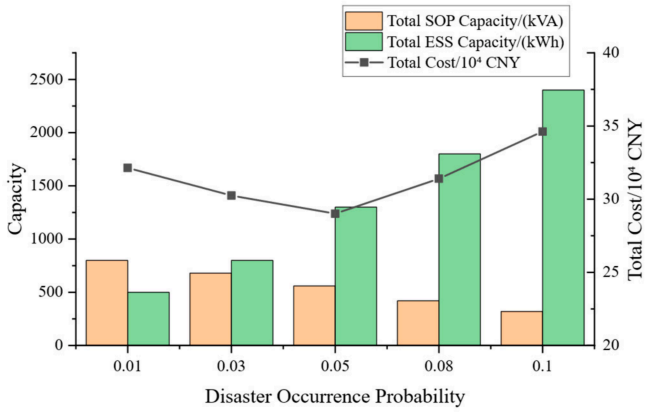


Figure 4. Sensitivity analysis of extreme disaster occurrence probability.

When extreme disasters occur rarely, the primary challenge faced by the system is spatial asymmetry under normal conditions; therefore, investment leans towards SOPs while significantly reducing ESS configuration. This is because SOPs can provide continuous benefits from network loss optimization and PV curtailment accommodation during normal operation, whereas the high initial investment of ESS struggles to yield returns under

low-frequency disasters. However, as the probability of blizzard disasters climbs to 0.10, the risk of topologically asymmetric breakage faced by the system increases sharply, leading to a fundamental reversal in the investment strategy: ESS capacity surges to 2500 kWh to ensure absolute active power support capability during the islanding period. This analysis demonstrates that the joint configuration model proposed in this paper can adaptively seek the optimal investment boundary between normal-state arbitrage and disaster mitigation based on the actual meteorological risk distribution of the region where the distribution network is located.

In the scenario generation phase of this model, sequential Monte Carlo sampling is adopted, which introduces random disturbances to the final planning decisions. To verify the solution stability and convergence robustness of the progressive hedging algorithm when coping with randomness, 10 independent and complete cycles of scenario sampling and model solving were conducted for the coordinated configuration scheme proposed in this paper. The statistical results indicate that the total lifecycle costs obtained from the 10 independent simulations exhibit a high degree of convergence stability. Detailed convergence statistical indicators are presented in Table 3.

Table 3. Statistical results of objective function convergence under independent random sampling simulations (Unit: $\times 10^4$ CNY).

Indicator	Cost
Minimum	28.85
Average	29.01
Maximum	29.22
Standard Deviation	0.11

As shown in Table 3, since the PH algorithm forces the decisions of individual independent asymmetric scenarios to gradually approach a global consensus through penalty multipliers, the algorithm can stably converge as long as the total number of Monte Carlo samplings W is sufficiently large. The extremely small standard deviation demonstrates that the optimization-solving framework proposed in this paper can effectively overcome the interference of random operators during the scenario generation process.

6.3. Analysis of Load Restoration Characteristics Under Extreme Disasters

To further verify the dynamic support capability of the flexible resource joint configuration strategy under extreme events, this section extracts a highly representative disaster scenario for analysis. It is assumed that the system is severely impacted by an extraordinary blizzard at time t = 3, and the main lines 2–3 and 6–26 of the distribution network experience simultaneous irreversible physical breakages. This causes a large-scale downstream area to lose main grid power support. Furthermore, due to traffic blockages caused by the disaster, the emergency repair and restoration window lasts up to 6 h.

At time t = 1 of the operational cycle, the blizzard disaster begins to strike, and the distribution management system synchronously obtains the spatial trajectory variations in the disaster center through the meteorological warning interface. From t = 1 to t = 3, as ice and snow continuously accumulate on the conductor surfaces, the physical stress of the lines begins to exhibit spatiotemporal asymmetry. Until t = 3, as the snow accumulation thickness breaks through the physical load-bearing limits, main lines 2–3 and 5–25 experience instantaneous and irreversible physical breakages. At this very moment, intelligent fault indicators deployed at critical network nodes capture the system fault, and the distribution management system precisely pinpoints the asymmetric fault sections where the topological breakage occurred.

After precisely identifying and isolating the fault locations, the system operator immediately initiates the post-disaster emergency network reconfiguration and multi-resource-coordinated regulation. At this time, the distributed energy storage systems deployed at nodes 17 and 32 respond instantaneously, rapidly transitioning to a V-*f* grid-forming control to establish stable voltage and frequency references for their respective de-energized islands. SOP 1 provides power support for node 7, restoring the power supply of the node 3–17 region. Concurrently, SOP 2 precisely transfers the surplus main grid energy, transferred via SOP 1 to node 17, across the tie line to the node 32 side to bear the intra-island load in coordination with DES 32. As a result, the distribution network continuously maintains the power supply for critical loads in the de-energized areas throughout the 6 h road-blocked emergency repair period.

The load restoration curves under different schemes are shown in Figure 5. The analysis results indicate that a distribution network relying solely on conventional network reconfiguration or the single configuration of SOPs cannot establish a stable islanded microgrid due to the lack of local active power support after the physical grid structure breaks, causing a large number of remote loads to fall into a prolonged power outage. Although the single configuration of DES can supply power to critical loads in the early stages of the disaster by relying on its energy, as the islanded operation time extends, the energy storage is highly prone to capacity depletion, thereby triggering secondary load shedding.

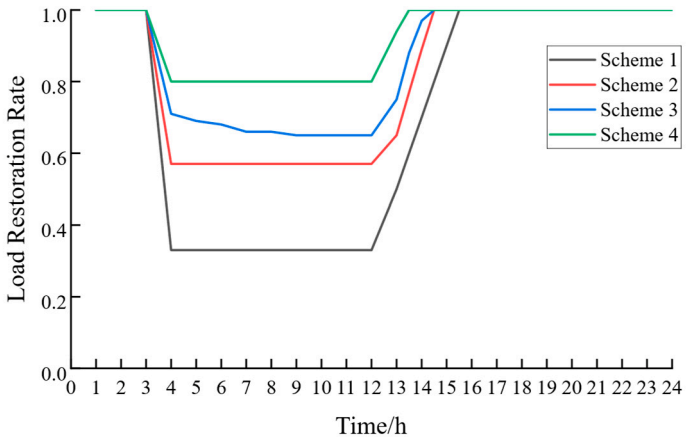


Figure 5. Comparison of load restoration curves under different schemes.

In contrast, the SOP- and DES-coordinated configuration strategy proposed in this paper enhances the resilience of the system. During the fault isolation and islanded operation stages, the DES utilizes the backup capacity reserved before the disaster to provide stable asymmetric voltage support for the loads; simultaneously, the SOP achieves symmetrical power sharing and power flow regulation among adjacent nodes. The synergistic effect of the two effectively overcomes the operational bottlenecks of single resources, minimizes the system's lost load amount under extreme disasters to the greatest extent, and realizes the effective enhancement of distribution network resilience.

To thoroughly reveal the underlying mechanism of the coordinated configuration strategy of SOPs and DES under extreme blizzard conditions, this paper provides an in-depth analysis of their operating states during the aforementioned disaster period. SOP and DES operating status are shown in Figure 6.

During the normal operation phase prior to the disaster, driven by the endogenous symmetric coupling constraint for the disaster state within the optimization model, the DES units at nodes 17 and 32 spontaneously curtailed their nighttime arbitrage behaviors. By reserving a certain margin for the initial state of charge (SOC), they built a solid pre-disaster

energy barrier. During the fault period, the DES rapidly transitioned to a V-f grid-forming control to provide local active power support, while the SOPs executed cross-area power transfer to prevent system voltage collapse. When entering the post-disaster clearing period, as the PV output at node 17 gradually recovered, the SOP rapidly switched to a full-load state, precisely transmitting the active PV power across the transformer areas to the heavily loaded node 32. This significantly alleviated the discharge pressure on the ESS at node 32, while the DES at node 17 absorbed the surplus power locally for charging.

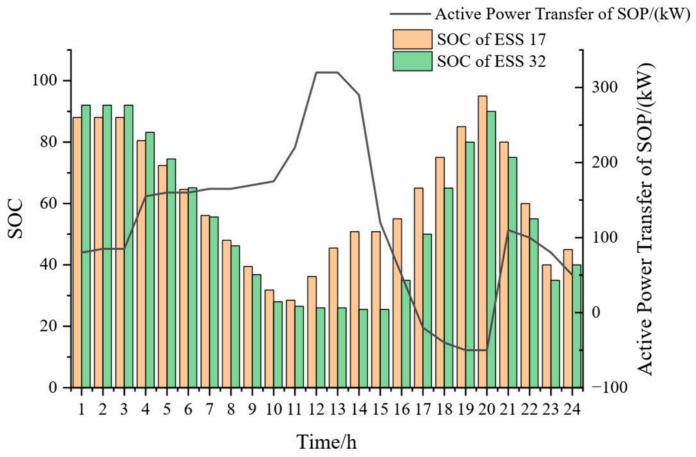


Figure 6. SOP and DES operating status.

6.4. Large-Scale System Scalability Analysis

To verify the applicability and scalability of the proposed method when facing large and complex networks, algorithm validation was conducted on the IEEE 123-node test system.

The topology of the modified IEEE 123-node test system is illustrated in Figure 7. The rated voltage of this test case is 4.16 kV, with a total active load of 3490 kW and a reactive power demand of 1920 kVar. Since the effectiveness of the schemes has been thoroughly verified using the 33-node system, this large-scale case study only compares the optimization results of Scheme 1 and Scheme 4, as shown in Table 4.

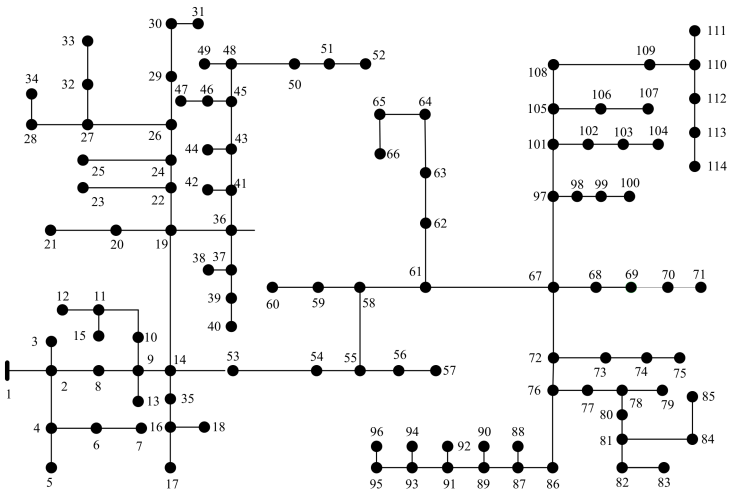


Figure 7. Topology of the IEEE 33-bus system.

In large-scale scenarios, the progressive hedging algorithm allocates a massive number of asymmetric scenarios to different computing threads for independent solving, enabling the model to stably converge within an acceptable time frame. As indicated by the load-

shedding penalties in Table 4, the resilience enhancement effect of Scheme 4 in the large network is even superior to that in the small-scale network. Furthermore, taking a disaster scenario where concurrent breakages occur on main line segments 67–97 and 61–67 under an extreme blizzard as an example, in Scheme 1, conventional reconfiguration easily leads to large-scale power outages due to the lack of local active power support; conversely, in Scheme 4, the algorithm deploys higher capacities of DES at the network edges, terminals, and core heavily loaded nodes, alongside the configured SOPs. When the disaster strikes, the cross-feeder transfer flexibility provided by the SOPs and the power support capability of the DES not only successfully suppress the expansion of the fault outage scope but also completely avert the risk of a total grid collapse in the 123-node system.

Table 4. Result comparison of different strategies under the IEEE 123-node system.

Configuration	SOP/DES	Cost				
		Configuration	Network Loss	PV Curtailment	Load Shedding	Total
Scheme 1	/	0	85.2	45.1	39.5	169.8
Scheme 4	SOP:55–94, 31–50 DES:53, 72, 108	16.3	32.15	18.6	8.45	121.5

7. Conclusions

This paper proposes an optimal configuration method for distributed energy storage and distribution network flexible interconnection devices, considering both operational economy and resilience enhancement, aiming to address the increasingly prominent multi-dimensional asymmetry challenges in modern power systems. First, a multi-dimensional scenario set encompassing the spatially asymmetric fluctuations of normal sources and loads and the spatiotemporally asymmetric evolution characteristics of extreme blizzards is constructed, accurately characterizing the multiple spatiotemporal uncertainties of the system. Second, a joint configuration model aimed at minimizing the total economic cost over the life cycle of planning and operation is established, constructing a symmetrical coupling mapping between normal and extreme conditions at the mathematical foundation. On this basis, the progressive hedging algorithm is introduced to break the decision-making asymmetric silos among a massive number of unanticipated scenarios, efficiently solving the model.

The case study verification results show that, compared to configuration schemes with a single flexible resource or no flexible resources, the joint coordinated configuration strategy proposed in this paper can effectively establish a symmetrical balance of spatiotemporal resources, avoid redundant investment in single devices, and significantly reduce network loss and PV curtailment penalties when the system deals with asymmetric power flows at a more reasonable cost. At the same time, when facing line-breakage faults with extreme topologically asymmetric breakage, the spatiotemporal synergistic effect of SOPs and distributed energy storage minimizes the system's lost load to the greatest extent. This fully verifies the superiority of this method in balancing operational economy and distribution network resilience enhancement while addressing multiple spatiotemporal asymmetric challenges.

Author Contributions: Conceptualization, S.Y.; methodology, G.L.; investigation, Z.W. and J.Z.; data curation, X.M. and W.L.; writing—original draft preparation, R.L.; writing—review and editing, J.W. All authors have read and agreed to the published version of the manuscript.

Funding: This research was funded by the Science and Technology Project of State Grid Jibei Electric Power Co., Ltd. Research on Flexible Interconnection Devices and Energy Storage Configuration

and Scheduling Technologies for Supporting Multi-State Efficient Operation of Rural Low-Voltage Distribution Networks, grant number B3018K24005U.

Data Availability Statement: Data are contained within the article. Further inquiries can be directed to the corresponding author.

Conflicts of Interest: Authors Saining Yin, Xinsheng Ma, and Weiyu Li were employed by the State Grid Jibei Electric Power Company Limited Electric Power Research Institute. Authors Guowu Li, Zezhong Wang, and Jin Zong were employed by the State Grid Jibei Electric Power Company Limited. The remaining authors declare that the research was conducted in the absence of any commercial or financial relationships that could be construed as potential conflicts of interest. The authors declare that this study received funding from Science and Technology Project of State Grid Jibei Electric Power Co., Ltd. The funder was not involved in the study design, collection, analysis, interpretation of data, the writing of this article or the decision to submit it for publication.

References

1. Wang, Y.; Chen, C.; Wang, J.; Baldick, R. Research on resilience of power systems under natural disasters—A review. *IEEE Trans. Power Syst.* **2015**, *31*, 1604–1613. [CrossRef]
2. Panteli, M.; Mancarella, P. The grid: Stronger, bigger, smarter?: Presenting a conceptual framework of power system resilience. *IEEE Power Energy Mag.* **2015**, *13*, 58–66. [CrossRef]
3. Panteli, M.; Pickering, C.; Wilkinson, S.; Dawson, R.; Mancarella, P. Power system resilience to extreme weather: Fragility modeling, probabilistic impact assessment, and adaptation measures. *IEEE Trans. Power Syst.* **2016**, *32*, 3747–3757. [CrossRef]
4. Jiang, X.; Zhou, Y.; Ming, W.; Yang, P.; Wu, J. An overview of soft open points in electricity distribution networks. *IEEE Trans. Smart Grid* **2022**, *13*, 1899–1910. [CrossRef]
5. Li, P.; Song, G.; Ji, H.; Zhao, J.; Wang, C.; Wu, J. A supply restoration method of distribution system based on soft open point. In *2016 IEEE Innovative Smart Grid Technologies-Asia (ISGT-Asia)*; IEEE: New York, NY, USA, 2016; pp. 535–539.
6. Bai, L.; Jiang, T.; Li, F.; Chen, H.; Li, X. Distributed energy storage planning in soft open point based active distribution networks incorporating network reconfiguration and DG reactive power capability. *Appl. Energy* **2018**, *210*, 1082–1091. [CrossRef]
7. Baghban-Novin, S.; Hamidi, A.; Golshannavaz, S.; Nazarpour, D. E-SOP's contribution in a techno-economic and clean operation of distribution networks: A multi-objective optimization approach based on linear models. *Int. Trans. Electr. Energy Syst.* **2020**, *30*, e12235. [CrossRef]
8. Zhang, T.; Wang, J.; Zhong, H.; Li, G.; Zhou, M.; Zhao, D. Soft open point planning in renewable-dominated distribution grids with building thermal storage. *CSEE J. Power Energy Syst.* **2020**, *9*, 244–253. [CrossRef]
9. Kabirifar, M.; Fotuhi-Firuzabad, M.; Moeini-Aghtaie, M.; Pourghaderi, N.; Dehghanian, P. A bi-level framework for expansion planning in active power distribution networks. *IEEE Trans. Power Syst.* **2021**, *37*, 2639–2654. [CrossRef]
10. Pamshetti, V.B.; Singh, S.P. Coordinated allocation of BESS and SOP in high PV penetrated distribution network incorporating DR and CVR schemes. *IEEE Syst. J.* **2020**, *16*, 420–430. [CrossRef]
11. Wang, H.; Wang, S.; Yu, L.; Hu, P. A novel planning-attack-reconfiguration method for enhancing resilience of distribution systems considering the whole process of resiliency. *Int. Trans. Electr. Energy Syst.* **2020**, *30*, e12199. [CrossRef]
12. Ma, S.; Li, S.; Wang, Z.; Qiu, F. Resilience-oriented design of distribution systems. *IEEE Trans. Power Syst.* **2019**, *34*, 2880–2891. [CrossRef]
13. Zhang, J.; Foley, A.; Wang, S. Optimal planning of a soft open point in a distribution network subject to typhoons. *Int. J. Electr. Power Energy Syst.* **2021**, *129*, 106839. [CrossRef]
14. Huang, Z.; Zhang, Y.; Xie, S. A comprehensive strategy for the distribution network resilience enhancement considering the time-varying behaviors of typhoon path. *Electr. Power Syst. Res.* **2023**, *214*, 108819. [CrossRef]
15. Ma, S.; Su, L.; Wang, Z.; Qiu, F.; Guo, G. Resilience enhancement of distribution grids against extreme weather events. *IEEE Trans. Power Syst.* **2018**, *33*, 4842–4853. [CrossRef]
16. Gilani, M.A.; Kazemi, A.; Ghasemi, M. Distribution system resilience enhancement by microgrid formation considering distributed energy resources. *Energy* **2020**, *191*, 116442. [CrossRef]
17. Ghasemi, M.; Kazemi, A.; Bompard, E.; Aminifar, F. A two-stage resilience improvement planning for power distribution systems against hurricanes. *Int. J. Electr. Power Energy Syst.* **2021**, *132*, 107214. [CrossRef]
18. Liu, G.; Jiang, T.; Ollis, T.B.; Li, Z.; Tomsovic, K. Resilient distribution system leveraging distributed generation and microgrids: A review. *IET Energy Syst. Integr.* **2020**, *2*, 289–304. [CrossRef]
19. Shi, Q.; Liu, W.; Zeng, B.; Hui, H.; Li, F. Enhancing distribution system resilience against extreme weather events: Concept review, algorithm summary, and future vision. *Int. J. Electr. Power Energy Syst.* **2022**, *138*, 107860. [CrossRef]

20. Ghosh, P.; De, M. Resilience-Oriented Planning for Active Distribution Systems. *Int. J. Electr. Power Energy Syst.* **2024**, *158*, 109976. [CrossRef]
21. Taheri, B.; Safdarian, A.; Moeini-Aghtaie, M.; Lehtonen, M. Distribution system resilience enhancement via mobile emergency generators. *IEEE Trans. Power Deliv.* **2021**, *36*, 2308–2319. [CrossRef]
22. Zhang, G.; Zhang, F.; Zhang, X.; Wang, Z.; Meng, K.; Dong, Z.Y. Mobile emergency generator planning in resilient distribution systems: A three-stage stochastic model with nonanticipativity constraints. *IEEE Trans. Smart Grid* **2020**, *11*, 4847–4859. [CrossRef]
23. Zhang, S.; Ge, S.; Liu, H.; Hou, G.; Wang, C. An analytical method for Delineating Feasible Region for PV integration capacities in net-zero distribution systems considering battery energy storage system flexibility. *J. Mod. Power Syst. Clean. Energy* **2024**, *12*, 475–487. [CrossRef]
24. Abu Saaklayen, M.; Liang, X.; Faried, S.O.; Martirano, L.; Sutherland, P.E. Soft Open Point-Based Service Restoration Coordinated with Distributed Generation in Distribution Networks. *IEEE Trans. Ind. Appl.* **2024**, *60*, 2554–2566. [CrossRef]

Disclaimer/Publisher's Note: The statements, opinions and data contained in all publications are solely those of the individual author(s) and contributor(s) and not of MDPI and/or the editor(s). MDPI and/or the editor(s) disclaim responsibility for any injury to people or property resulting from any ideas, methods, instructions or products referred to in the content.